

Performance Characteristics of Non-Arc Double Stator Permanent Magnet Generator

R. Suhairi^{1, 2, 3}, R. N. Firdaus^{1, 2, *}, M. Z. Aishah^{1, 2}, F. Azhar^{1, 2},
M. N. Othman^{1, 2}, Z. Ibrahim¹, and C. V. Aravind⁴

Abstract—The improvement in the power density in the double stator configurations is feasible with increase in the electrical loading of the electrical machines. This type of newer configuration is finding significant applications in improvising energy generation, more commonly for renewable energy generation. Various double stator configurations with non-arc permanent magnet machines for power density are modelled and analyzed in this paper. Finite Element Method (FEM) is used to simulate for the generation capability including the electromagnetics parameters such as flux linkage and open circuit voltage. A new slotted rotor structure is evolved based on the magnetic flux flow control inside the machine. The proposed structure is then fabricated in the laboratory and tested for operating characteristics with load circuit. The proposed machine produces a maximum power of 600 W at speed of 2000 rpm with 75% of maximum efficiency with the micro-hydro generation unit.

1. INTRODUCTION

Generation of electricity is challenged by the reduction in the availability of the natural resources around the globe. The generation of electrical power needs to be increased rapidly due to the various forms of energy requirement to support the global demand. Generally, electrical generator is a device that converts mechanical energy obtained from an external source into electrical energy. The source of the mechanical power could be of diesel engine, steam turbine, water turbine, or any similar device [1]. Structural variations of the electromechanical devices through magnetic flow control are proposed by several researchers through dual magnetic circuit inclusive double stators [2–7] and double rotors [8, 9]. In 2005, Feng et al. designed a double-stator starter generator for a hybrid vehicle to increase the performance per volume and performance cost ratio [2]. In 2006, Chau et al. designed and analyzed a doubly-salient permanent magnet machine with a new outer-rotor with the capability of flux control [3]. In 2008, Liu et al. designed and fabricated a new outer-rotor permanent magnet hybrid machine for wind generation, where the machine with a two-excitation permanent magnet and a Direct Current (DC) field winding in order to maintain constant output voltage at a wide range of speeds and currents [4]. Norhisam et al. [5] developed a single-phase permanent magnet generator to obtain high output power and high efficiency, and the slot pole combination and length of the outer stator yoke of the generator are varied to find best possible configurations. Reference [7] presents comparative evaluations on the power density of several types of double-stator slot and slot-less topologies of Permanent Magnet Generator (PMG) which are purposely designed for agriculture sectors. This double-stator topology maximizes the usage of flux linkage that leads to high power density [10–12]. In [13], a new structure for a double-stator brushless DC motor with thick pole shoe with improved energy density compared to conventional

Received 15 November 2016, Accepted 30 December 2016, Scheduled 1 February 2017

* Corresponding author: Raja Nor Firdaus (norfirdaus@utem.edu.my).

¹ Faculty of Electrical Engineering, Universiti Teknikal Malaysia Melaka (UTeM), Hang Tuah Jaya, Durian Tunggal, Melaka 76100, Malaysia. ² Electrical Machine Design, Power Electronics and Drives Research Group, CeRIA, UTeM, Hang Tuah Jaya, Durian Tunggal, Melaka 76100, Malaysia. ³ Universiti Kuala Lumpur-British Malaysian Institute, Gombak, Selangor 53100, Malaysia. ⁴ School of Engineering, Taylor's University, Malaysia, Subang Jaya 47100, Malaysia.

structure is introduced with the limitations on the research covering the single phase topology. A three-phase double-stator cup-shaped rotor for wind power generation with optimal pole-to-slot ratio produces low torque ripple [14]. A three-phase generator with a permanent magnet mounted on both the inner and outer surfaces is proposed in [15]. It reduces the length of the magnetic path that saves the iron yoke material resulting in increased power output. In [16], the use of concentrated winding arrangement avoids the end winding losses, and thereby the copper losses are reduced with an increase in the performance of the machine.

Most of the research mentioned above studied double stators for power density approach for the conventional power generation strategy, but operation at variable and low speed condition such as micro-hydro application is not attempted. In addition, the main constraint in double-stator topology is to maintain its mechanical air gap between the inner and outer stator configurations. The mechanical air gap is to be as small as possible or at the same size with electromagnetic air gap in order to maximize usage of the flux generated by the winding coil and permanent magnet. Also in the double-stator topology, arc-shaped permanent magnet is popular due to the rotor being positioned between two stators. Nevertheless, the arc permanent magnet is not economical [7], and a new rotor design that uses a rectangular shape permanent magnet with the smallest electromagnetic air gap makes it more advantageous for the double-stator topology.

Therefore, this research investigates and studies the performance of non-arc of several models of available DSPMG with different rotor structures for the flux linkage and electro-motive force. Several topologies such as Double Stator Interior Permanent Magnet Generator (DSI-PMG) [17], Double Stator Spoke Type Permanent Magnet Generator (DSST-PMG) [18], and Double Stator Double Pole Permanent Magnet Generator (DSDP-PMG) [5] are modeled, simulated and analyzed. A newer rotor with slotted configuration is introduced as a Double Stator Slotted Rotor Permanent Magnet Generator (DSSR-PMG) and is compared with the above three structures. The salient feature of the proposed DSSR-PMG is that it has minimum electromagnetic air gap where all the generated flux is optimized and evenly distributed at the stator-air gap in order to avoid the leakage flux. The developed DSSR-PMG increases output power and efficiency when it is tested with the load circuit.

2. APPLICATION OF RESEARCH

This research is aimed to study the best possible PMG configuration for micro-hydro applications in Malaysia. The energy challenge in Malaysia is addressed with this micro-hydro technology with the use of higher grounds most particular in rural areas [19]. However, only slightly higher are discovered such as typical small lake or water drain in the city. Currently for the testing purposes and applications of the PMG, the water wheel system developed by the University Teknikal Malaysia Melaka (UTeM) in real scale as shown in Figure 1(a) is used. The water wheel system is driven by water from the lake that enters through a pipeline into a fiber water bucket placed around the wheel. Due to the accumulated water in the bucket, the water wheel spins and rotates the shaft and is connected to the gear system and the PMG. There are two PMGs attached at the left and right sides of the water wheel.

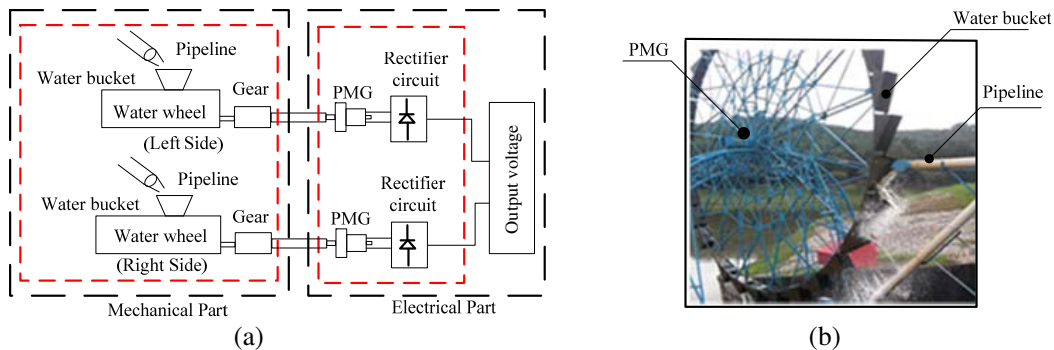


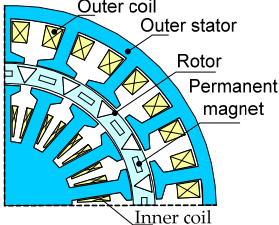


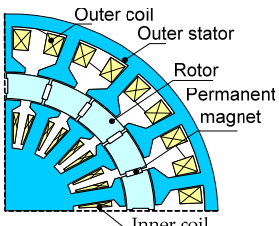


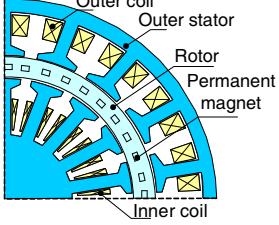
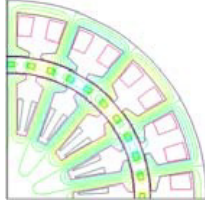
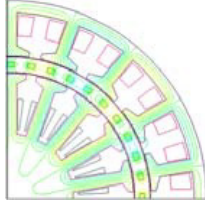
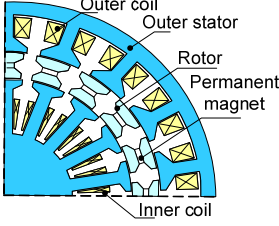


Figure 1. Block diagram and water wheel system. (a) Block diagram. (b) Water wheel system.

The generated AC output voltage is modulated to become unidirectional with the aid of the rectifier circuit making it become storage capable DC voltage. This system is separated with two parts. The first part is mechanical part which consists of water bucket to receive the amount of water flow from the pipeline. The water wheel system as shown in Figure 1(b) rotates at optimum speed of 10 rpm; the PMG operates at speed of 2000 rpm. A gear is used to convert the rotation of the wheel and attached to the water wheel to increase the speed of PMG. The second part is electrical part which consists of PMG that generates the output power and rectifier system for the desired output voltage.

3. STRUCTURAL COMPARISON

All the three types of generators, the DSDP-PMG, DSSM-PMG and DSI-PMG, with different rotor structures already in place and the new Double Stator Permanent Magnet Generator with Slotted Rotor (DSSR-PMG) are modeled, simulated and analyzed for the flux lines, flux density and rotor parameters which are also presented in Table 1 with brief description of each of those.

Table 1. Machine configurations, magnetic flux and rotor parameters.

DSI-PMG			
DSST-PMG			
DSDP-PMG			
DSSR-PMG			

3.1. Double Stator Interior Permanent Magnet Generator (DSI-PMG)

The design of the rotor for DSI-PMG structure consists of non-ferromagnetic material and permanent magnet. The rotor is cup-shaped with a mechanical air gap between permanent magnet and stator of 3.5 mm in the outer and inner stators. There is a significantly large air gap due to the rotor being made of non-ferromagnetic material, thereby the flux is not evenly distributed as shown in Table 1.

3.2. Double Stator Spoke Type Permanent Magnet Generator (DSST-PMG)

Spoke type permanent magnet machine is widely used in industry application [20–22]. DSST-PMG has a rotor structure of interior type permanent magnet with higher saliency ratios since it is made up of ferromagnetic material and usually used in high speed applications because permanent magnet is embedded in the rotor. It means that the magnetic flux generated by permanent magnet arrangement of spoke type is highly concentrated in air gap and produces high power density compared to that of the other PMG [23, 24]. In DSST-PMG, the end effect limits the voltage generation.

3.3. Double Stator Double Pole Permanent Magnet Generator (DSDP-PMG)

In this generator, permanent magnet is magnetized in the circumferential direction and surface-buried in the rotor for high speed application. The magnets are located between wedges of magnetic material of the pole pieces in the rotor. The connection of inner and outer stators is in series winding with the flux direction of the air gap in the radial direction. The flux lines and flux density are not evenly distributed at the rotor and permanent magnet due to the larger air gap in the inner stator and outer stator. The air gap for this model is 2.5 mm for each air gap and in total 5 mm air gap.

3.4. Double Stator Slotted Rotor Permanent Magnet Generator (DSSR-PMG)

This generator uses the radial flux flow inside the machine with the stator consisting of two parts and a rotor. The stator is composed of a coil and stator yoke for stator winding availability. The rotor structure is formed by a permanent magnet, rotor core, and shaft. The mechanical air gap between the outer and inner stators is 0.5 mm. The DSSR-PMG has permanent magnet volume and coil turns for inner and outer stators, which are 630 mm^3 and 110 turns.

The outer and inner diameters of the motor are 156 mm and 86 mm, respectively. The flux lines show that the flux is evenly distributed along the stator and permanent magnet thus maximizes the usage of flux. The flux density limitation of this model is about 1.5 T well below the saturation limit of 2.0 T.

3.5. Analysis Parameter

The total number of turns for all slots, number of slots and poles, number of phases and air gap between outer and inner stators, stack length, total volume of the permanent magnet and size used are set to specific values as shown in Table 2. The entire machine configuration is modeled and simulated by using comprehensive electromagnetic field simulation software (Ansys Maxwell) to analyze its electromagnetic performance. The rotor dimensions for the configurations are slightly different as shown in Table 3.

Since the rotor sizes for all models are not same, the slot space in outer and inner stators is varied depending on the rotor structure. This is to maintain the same air gap for both the inner and outer stators. The reason to maintain the mechanical air gap is to make sure that all models are fairly compared. There are four types of PMG with different rotor structures that are compared, namely, Double Stator Interior Permanent Magnet Generator (DSI-PMG), Double Stator Double Pole Permanent Magnet Generator (DSDP-PMG), Double Stator Spoke Type Permanent Magnet Generator (DSST-PMG) and the new Double Stator Permanent Magnet Generator with Slotted Rotor (DSSR-PMG).

The heights of inner and outer coils are changed due to the design variations on the rotor structure. The electromagnetic air gap in outer and inner stators is also changed due to the rotor configurations. For DSST-PMG and DSSR-PMG, the electromagnetic air gap is 0.5 mm, each at inner and outer peripheries since the rotor is made from ferromagnetic material to hold the permanent magnet. Besides,

Table 2. Specific parameter for all models.

Item	Element	Value
Outer stator	Outer stator diameter	156 mm
Number of turns	Outer stator	55 turns
	Inner stator	55 turns
Number of slots	18	
Number of poles	20	
Number of phase	3	
Permanent magnet volume	$6.3 \times 10^{-7} \text{ m}^3$	
Permanent magnet size	6 mm \times 2 mm \times 52.5 mm	
Coil size	0.6 mm	
Stack length	52.5 mm	
Outer air gap	0.5 mm	
Inner air gap	0.5 mm	

CPU: Intel Core i7 3.6 GHz, MEM: 32 GB

Table 3. Rotor parameter for all models.

Parameters	Machine configurations			
	DSI-PMG	DSST-PMG	DSDP-PMG	DSSR-PMG
Outer stator inner diameter, \varnothing_{osi} (mm)	108	110	112	112
Inner stator outer diameter, \varnothing_{iso} (mm)	86	88	98	94
Rotor outer diameter, \varnothing_{ro} (mm)	107	109	111	111
Rotor inner diameter, \varnothing_{ri} (mm)	87	89	99	95
Inner mechanical air gap (mm)	3.5	0.5	2.5	0.5
Outer mechanical air gap (mm)	3.5	0.5	2.5	0.5

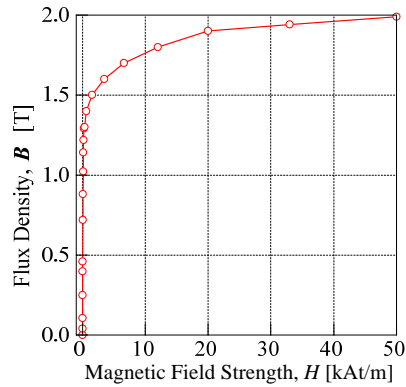
DSI-PMG and DSD-PPMG are with electromagnetic air gaps of 3.5 mm and 2.5 mm, respectively. Larger electromagnetic air gaps in DSI-PMG and DSDP-PMG compared to DSSR-PMG and DSST-PMG are due to the rotor material for DSI-PMG and DSDP-PMG rotor being made up of non-ferromagnetic material. This ferromagnetic and non-ferromagnetic materials are used for the rotor configurations based on the previous research.

Different types of material used for the rotor change the magnetic flux flow and flux density of the PMG in the air gap. There are two air gaps in the double stator configurations which are inner and outer air gaps. Based on the previous research, larger electromagnetic air gap also affects the overall performance of the PMG. The rotor material configuration for all models of PMG is shown in Table 4. The total numbers of turns for all the configurations and the total volume of PM are kept at $55 \times 10^{-7} \text{ m}^3$ and $6.3 \times 10^{-7} \text{ m}^3$, respectively. This is to ensure that the energy densities produced by all the machine configuration are the same.

Figure 2 shows the B-H curve of ferromagnetic material (Non-oriented silicon steel M250-35A). It shows that for ferromagnetic materials the ratio of flux density to field strength (B/H) is not constant but varies with flux density. The flux density increases in proportion to the field strength until it reaches a certain value if it cannot increase any more becoming almost level and constant as the field strength continues to increase. The flux density maximum limit or being saturated for this material is at about 2 Tesla which is higher than flux density of the designed PMG which is only limited at 1.5 Tesla. However, for non-ferromagnetic material, Acrylonitrile Butadiene Styrene C-11-01 (ABS) is considered as a constant, and this constant is known as μ_o , the permeability of free space, ($\mu_o = 4\pi \times 10^{-7} \text{ H/m}$) since the material is plastic.

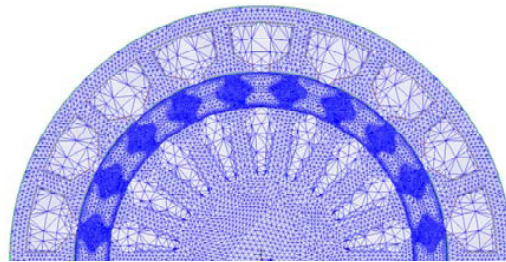
Table 4. Rotor material configurations for PMG.

Parameters	Rotor material configurations			
	DSI-PMG	DSST-PMG	DSDP-PMG	DSSR-PMG
Ferromagnetic (Non-oriented silicon steel M250-35A)		✓		✓
Non-ferromagnetic (Acrylonitrile Butadiene Styrene (ABS) C-11-01)	✓		✓	

**Figure 2.** B-H curve of M250-35A.

3.6. Flux Linkage and No-Load EMF

Due to model complexity, this research uses Finite Element Method (FEM). FEM provides magnetic analysis with high accuracy because it gives an approximation on a microscopic scale. However, it requires structure modeling and high memory capacities of computer, which in the end gives more drawback in computational time. It is clear that the adequacy of meshing directly affects the precision of computation [25–27]. The mesh model for DSSR-PMG is shown in Figure 3. The mesh is generated based on the specified maximum length of the triangle formed on the surfaced of the PMG. All the parameters for the boundary condition and geometrical description are shown in Table 5.

**Figure 3.** The mesh generated in DSSR-PMG.

All of these drawbacks are taken into account in this research to ensure reliability and accuracy. The FEM is used as a tool to obtain the result based on the basic calculation theoretically. The transient solver allows analysis on the magnetic fields and flux of a model at various time steps of a solution over a specified period of time. This solver allows for non-sinusoidal current or voltage excitation, as well as rotational motion. To compute the magnetic flux linkage, the FEM solver uses the following equation:

$$\phi = \int B \cdot dA \quad (1)$$

Table 5. Rotor material configurations for PMG.

Mesh Parameter		Value
Band	[mm]	0.5
Coil	[mm]	6.15
Magnet	[mm]	1.5
Rotor	[mm]	2
Stator	[mm]	6
Rotor and Stator	[mm]	2
Surface approximation for magnet	[mm, deg]	0.03, 15
Surface approximation for rotor and stator	[mm, deg]	0.06, 15

where B is the magnetic flux density and A the area over which flux density is computed. The DSSR-PMG has flux linkage at the inner and outer stators. The total flux linkage is the combination of flux linkage at inner and outer stators and is expressed as in Equations (2)–(4)

$$\phi_{inner_n} = N_{coil_inner} \times \omega_r \times A_{coil_inner} \times S_{coil_inner} \tag{2}$$

$$\phi_{outer_n} = N_{coil_outer} \times \omega_r \times A_{coil_outer} \times S_{coil_outer} \tag{3}$$

$$\phi_{phase_n} = \phi_{outer_n} + \phi_{inner_n} \tag{4}$$

where ϕ_{inner_n} is the flux linkage of inner stator [Wb], ϕ_{outer_n} the flux linkage of outer stator [Wb], ϕ_{phase_n} the total flux linkage per phase. The net flux linkage inside the machine includes the flux linkage of the outer and inner stators with that of the rotor in Equations (1) and (2) [Wb], and N_{coil_inner} is the total number of coil turns of inner stator in one phase, N_{coil_outer} the total number of coil turns of outer stator in one phase, ω_r the speed of the PMG [rad/s], A_{coil_inner} the area of single inner coil [m³], A_{coil_outer} the cross sectional area of single outer coil [m²], S_{coil_inner} the number of coil slots per phase of inner stator, and S_{coil_outer} the total number of coil slots per phase of the outer stator. The relationship between the flux linkage and the no-load EMF is as in Equations (5)–(7).

$$E_{inner_n} = \frac{d\phi_{phase_inner}}{dt} \tag{5}$$

$$E_{outer_n} = \frac{d\phi_{phase_outer}}{dt} \tag{6}$$

$$E_{phase_n} = E_{outer_n} + E_{inner_n} \tag{7}$$

where E_{inner_n} is the no-load EMF at the inner stator in [V], E_{outer_n} the no-load EMF at the outer stator in [V], and E_{phase_n} the total of inner and outer EMF for one phase in [V]. In the design process,

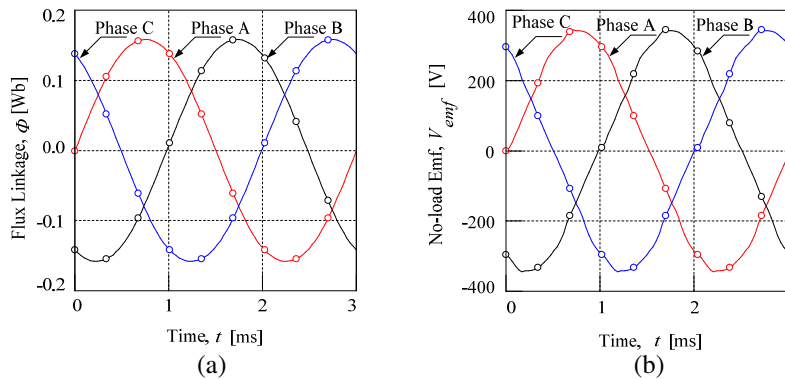


Figure 4. No-load EMF and flux linkage for DSSR-PMG at speed 2000 rpm. (a) Flux linkage. (b) No-load EMF.

the maximum value of flux density allowed for is 1.5 T in order to relieve the core saturation which is saturated at 1.8 T. In 2D FEM, all the models take the saturation effect and loss into account. Also in design and simulation, the values of flux linkage, back-EMF, flux density, flux lines and cogging torque have been taken iteratively by analytical design from the FEM simulation with high accuracy.

Figure 4 shows an example of simulation results of the magnetic flux linkage and no-load electromotive force (EMF) using FEM for three-phase DSSR-PMG configuration at constant speed of 2000 rpm (no load). The result of magnetic flux linkage and the no-load EMF are calculated in both the inner and outer stators. The ideal sinusoidal waveform of magnetic flux linkage shows the symmetry between phases and reflecting sinusoidal of the no-load EMF waveform. In the simulation, the peak value of the magnetic flux linkage is 0.158 Wb at rated speed of 2000 rpm as shown in Figure 4(a), while in Figure 4(b), the no-load EMF or no-load voltage is nearly 300 V per phase for the same speed.

3.7. Comparison of Flux Linkage and No-Load EMF

Figure 5 shows comparison of flux linkage and no-load EMF for the machine configuration. The simulation is run for speed from 500 rpm to 4000 rpm with all configurations under investigation. As seen in Figure 5(a). It is observed that the highest flux linkage is 0.158 Wb for the DSSR-PMG. Meanwhile, for both DSDP-PMG and DSI-PMG, the flux linkage is almost similar to the maximum value of 0.053 Wb and 0.05 Wb, respectively.

The DSST-PMG exhibits the lowest magnetic flux linkage of 0.015 Wb. The percentage differences between DSSR-PMG with DSDP-PMG and DSI-PMG are about 66% and 68%, respectively. The magnetic flux linkage of DSSR-PMG is 77% higher than that of the DSST-PMG. Since the magnetic flux linkage of the DSSR-PMG shows the highest value, the no-load EMF for this configuration contributes the highest value as shown in Figure 5(b), which shows that the EMF for DSSR-PMG is slightly higher than other models where maximum no-load EMF reaches 325 V for 3500 rpm.

For DSDP-PMG and DSI-PMG, the no-load EMFs are 125 V and 115 V, respectively. The no-load EMF is the lowest for DSST-PMG which is 55 V at maximum speed. There is significant difference in no-load EMF between DSSR-PMG and DSST-PMG wherein the DSSR-PMG configuration generates no-load EMF six times greater than DSST-PMG. In summary, the magnetic flux linkage and no load EMF are plotted to choose the best configuration, and it is inferred from the above analysis that the DSSR-PMG is the suitable one with highest values of flux linkage and no-load EMF.

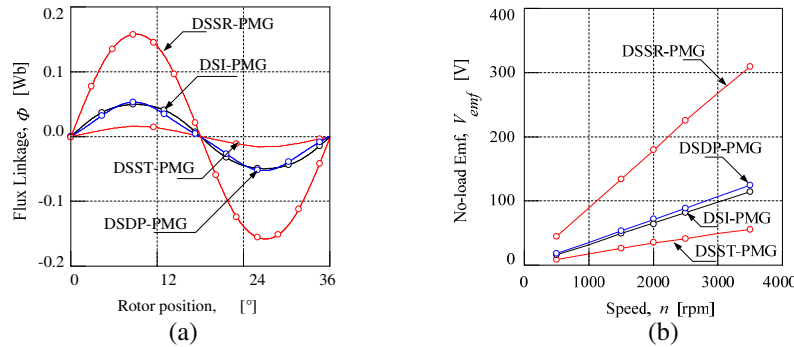


Figure 5. Flux linkage and average no-load EMF for all compared models. (a) Flux linkage. (b) No-load EMF.

4. RESULT AND DISCUSSION

Based on the numerical design analysis, a prototype of DSSR-PMG is fabricated to test its performance under laboratory conditions as shown in Figure 6.

The structural configuration of the fabricated machine is shown in Figure 6(a), and the cross-sectional structure of the fabricated machine is shown in Figure 6(b). The rotor, outer stator and inner stator are made from non-oriented silicon steel M250-35A with the lamination thickness of 0.35 mm

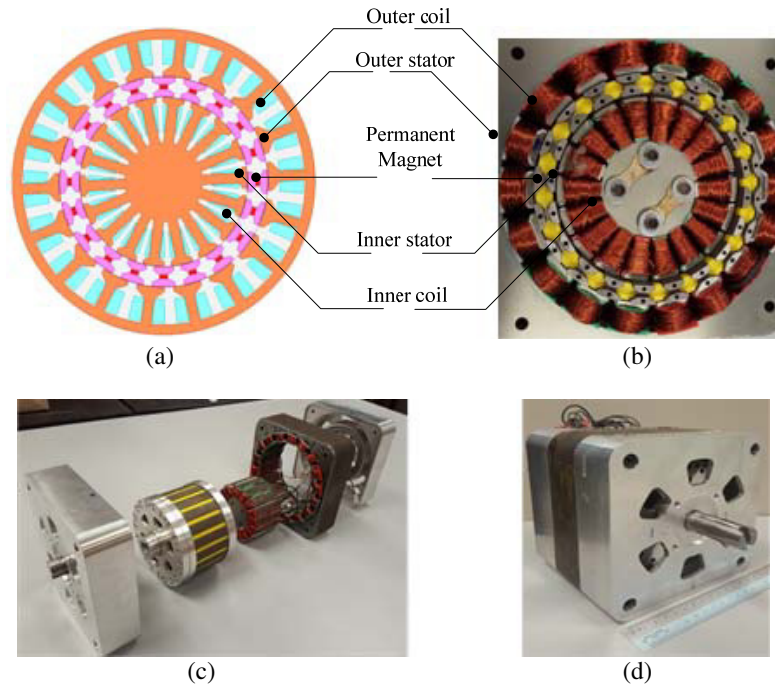


Figure 6. Prototype of DSSR-PMG. (a) Structural configuration of the DSSR-PMG. (b) Cross-sectional view. (c) Exploded view DSSR-PMG. (d) Assembled DSSR-PMG.

each. A slotted rotor with non-arc permanent magnets is embedded between the pole shoes. The fillers (marked yellow colors) in the Figure 6(b) are made from ABS material and placed between the rotor slots to give the required mechanical strength. This prevents the permanent magnet from being displaced from its original position as it is designed for high speed applications. The PM used is made from Neodymium Boron Iron (NdFeB42) with a dimension of 2 mm width and 6 mm height and length 52.5 mm. The 0.6 mm diameter size of coil is used for winding in the outer and inner stators. The inner and outer stators are connected in series with concentrated winding configurations. The stack length and air gap lengths between inner stator-rotor and outer stator-rotor are set for 52.5 mm and 1 mm, respectively. The coil case is slotted to all the stator teeth to prevent short circuit between coils and stators during winding process. Bearings are placed at the front and back casings to mount the rotor to give stability and strengthen to the rotor rotating at high speed. There are small holes designed at the front and rear casings of DSSR-PMG in order to release heat from the DSSR-PMG during the operation of the machine. Figure 6(c) shows the exploded view of the fabricated DSSR-PMG, and Figure 6(d) shows the assembled prototype used for experimental work.

4.1. Experimental Setup

Figure 7(a) and Figure 7(b) show the block diagram and experimental setup for measurement validation. The fabricated DSSR-PMG is attached to the jig with instrumentation system for measurements. The prime mover for the DSSR-PMG is a 3-kW High Power Brushless DC motor with fan cooling (Model: HPM03KW-10D-PZ) powered from battery bank with capacity of 48 V. The speed of the prime mover is controlled by throttle that comes with the vector control driver (Model: 48V240L). The maximum speed of the prime mover at full load is 4000 rpm. As the prime mover rotates, the voltage is induced in DSSR-PMG and recorded through the oscilloscope. The current and voltage sensor probes (Model: A622 AC/DC Current Probe) are coupled with the 4.5 kW Programmable AC/DC Electronic load (Model: Chroma 63804). The generated output voltage and current from the DSSR-PMG are rectified by the full bridge rectifier circuit before being connected to the adjustable resistive electronic load. The DC voltage and current with the real power are displayed at the electronic load, and the V-I waveforms are captured by oscilloscope and recorded and saved to the laptop for further performance

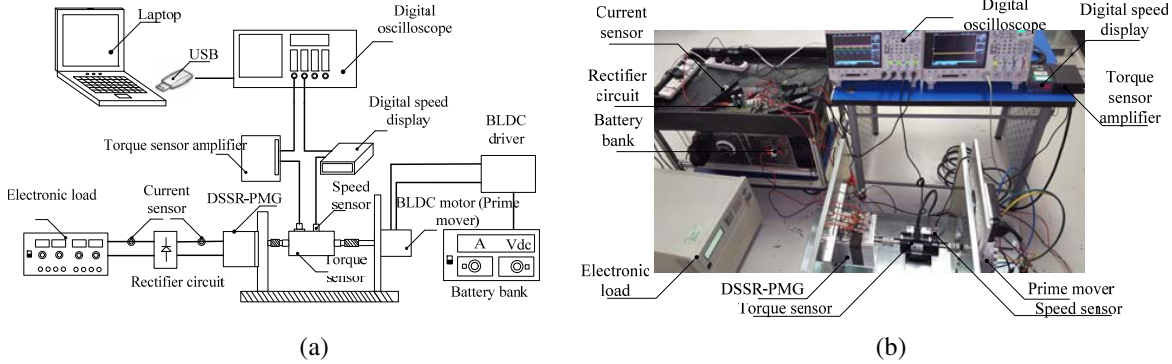


Figure 7. Experimental setup. (a) Block diagram for experimental setup. (b) Actual measurement.

analysis process. The load is varied from $10\ \Omega$ to $100\ \Omega$ in order to evaluate the performance of the DSSR-PMG at various speeds. The mechanical torque produced by the prime mover required to rotate the DSSR-PMG is recorded by the torque sensor and amplified by using an amplifier. The speed of the DSSR-PMG is captured through a Digital Speed Display. All the parameter values such as torque, speed, voltage and current are used for analysis proposes.

4.2. Validation Results

Figure 8(a) shows the simulation and measurement results of no-load EMF for operating speed of 2000 rpm. It is seen that the peak value of EMF in simulation is 320 V and is of nearly sinusoidal waveform. On the other hand, for experiment, the peak value is dropped by 20 V which is only 300 V compared to simulation or 6.25% percentage difference expected. The no-load EMF characteristics of both the analytical and experimental results are in good agreement as seen in Figure 8(a). The average no-load EMF is proportional to the speed of DSSR-PMG, and the average EMF produced by the DSSR-PMG is 319.7 V at the speed of 3500 rpm. In FEM simulation, the maximum EMF at the same operating speed is 325 V which is 1.63% in difference compared to that of the measurement. At the rated speeds of 2000 rpm, the average EMFs from FEM simulation and experiment are 181 V and 178 V, respectively. It can be concluded that the simulations results are valid and acceptable, and agree with that of the measurement ones. Hence, the performance of DSSR-PMG through flux linkage maximization enhances voltage generation in comparison with other existing models in the literature.

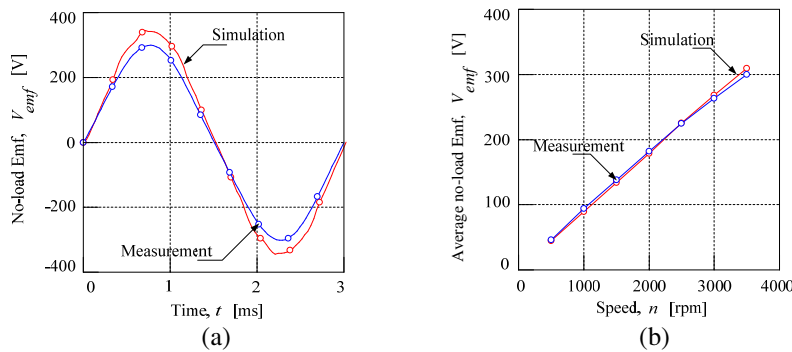


Figure 8. FEM simulated and experimental results of DSSR-PMG. (a) No-load EMF at 2000 rpm. (b) Average no-load EMF at various speed.

4.3. Performance Analysis of DSSR-PMG

In order to estimate the performance of the DSSR-PMG with the prime mover torque, input power, mechanical power and efficiency, FEM-Analytical method is used. FEM-Analytical is a method that

combines simulation and mathematical approach to determine specific dynamic value of the generator. The output voltage and output current of the generator are simulated by FEM based on the external circuit as shown in Figure 9. Here, the losses calculation such as the core, hysteresis and eddy current losses are considered by FEM. The DSSR-PMG is designed to operate at rated speed of 2000 rpm.

The output of the generator in wye-connection is rectified and connected to resistive load of 100 Ω. The input power which is the mechanical power from the prime mover motor that rotates the PMG is calculated using Equation (7).

$$P_m = \frac{2\pi \times T \times n}{60} \text{ [W]} \tag{8}$$

where P_m is the mechanical power by the machine in [W] that acts as a prime mover, T the torque [Nm], and n the rotational speed in [rpm].

The measured output power of the generator is measured at the load using Equation (8). The output voltage and current are captured using an oscilloscope whereas V is the DC output voltage [V], and I is the DC output current [A]. The efficiency, η , is calculated by the percentage ratio of output power to the input power which is the mechanical power as shown in Equation (9). The efficiency indicates the optimum value of power used and converted rightfully to the desired output.

$$P_o = V \times I \text{ [W]} \tag{9}$$

$$\eta = \frac{P_m}{P_o} \times 100 \text{ [%]} \tag{10}$$

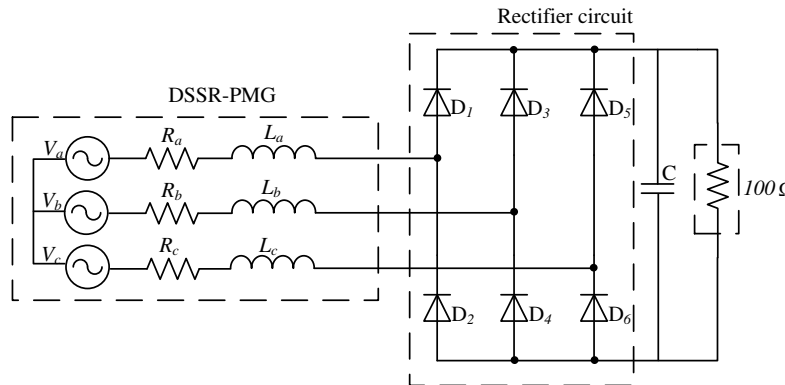


Figure 9. Load circuit with the PMG.

Figure 10 shows the performance analysis of DSSR-PMG. It is seen from Figure 10(a) that the torque of the generator is increased from 2.5 Nm up to 4.5 Nm for speed from 500 rpm to 1500 rpm until it starts to saturate. The results for FEM-analytical and measurement are in close agreement. The value of 4.5 Nm is considered lower for a micro-hydro application. This shows that the DSSR-PMG does not require higher torque at prime mover for generation of electricity. Figure 10(b) shows the mechanical power of the DSSR-PMG at various speed conditions. The result shows that the mechanical power is increased as the speed increases.

The highest mechanical powers recorded by the FEM-analytical and measurement are 1400 W and 1500 W, respectively. There are small significant differences between the FEM-analytical and measurement results of the mechanical power. Figure 10(c) shows the output power of DSSR-PMG via rectified load. It is seen that the output power is gradually increased as the speed increases for both air gaps at inner and outer stators. As the DSSR-PMG rotates, the voltage induced is measured in the load with the output power of 1000 W for measured speed at 3500 rpm. In addition, the output power is about 650 W at rated speed of 2000 rpm.

Furthermore, the value computed through the FEM-analytical gives small significant difference from that of the measurement results. The efficiency of DSSR-PMG is shown in Figure 10(d). The efficiency is 75% at the rated speed of 2000 rpm for both FEM-analytical and measurement results. The maximum efficiency is measured for a speed of 1500 rpm around 77%. It is seen that the efficiency

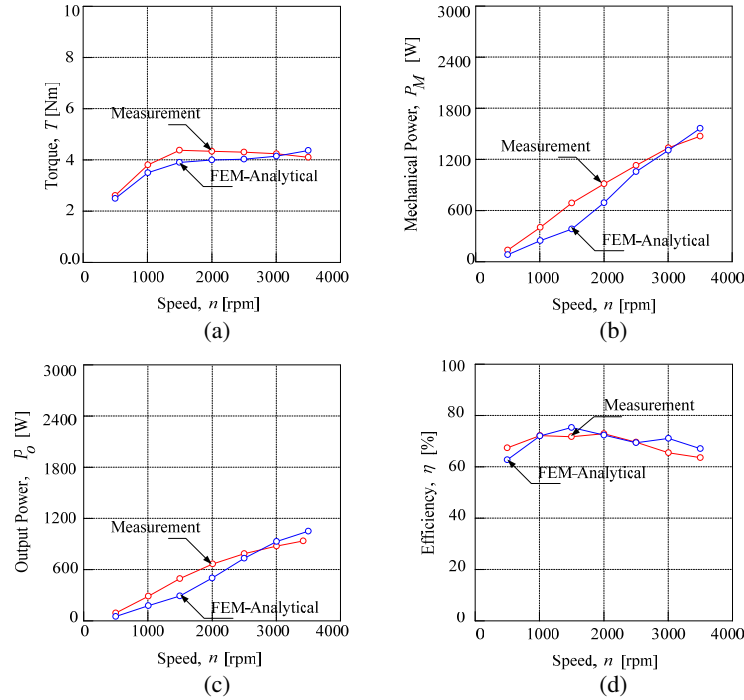


Figure 10. Performance characteristic. (a) Torque. (b) Mechanical power. (c) Output power. (d) Efficiency.

value of DSSR-PMG is consistent between 60% and 77%. The consistency of the efficiency curve gives advantages to the DSSR-PMG to operate at variable speed range of 1000 rpm to 2000 rpm. Thus, it is shown that DSSR-PMG topology is suitable for renewable energy application such as the micro-hydro applications.

5. CONCLUSION

In conclusion, several types of double-stator configurations are modelled and compared in this research for the power generation in micro-hydro applications. The Double Stator Permanent Magnet Generator with Slotted Rotor (DSSR-PMG) has the highest flux linkage and EMF compared to DSDP-PMG, DSST-PMG, and DSI-PMG which are 66%, 68%, 77% and 61%, 64%, 83%, respectively. The DSSR-PMG is fabricated for performance analysis in term of output power and efficiency. Thus, the structure of DSSR-PMG with electromagnetic air gap provides a large significant effect to the performance of the generator. This is due to higher flux linkage thus, induced higher voltage and current which contribute to the output power of the generator. The DSSR-PMG topology shows consistent efficiency value with the maximum efficiency 75%. The implementation of the slotted rotor allows magnetic flux to be optimized and evenly distributed at the air gap of the inner and outer stators, thus this DSSR-PMG has a potential for the use as a micro-hydro generation. A good agreement in results between simulation and experiment is achieved in order to prove the accuracy of simulation results in FEM and data taken during experimental work. The study on thermal analysis will be done and reported in the near future together with that of electro-mechanical and electro-magnetic analysis for all the models of DSDP-PMG, DSI-PMG and DSST-PMG.

ACKNOWLEDGMENT

The authors would like to thank Ministry of Education Malaysia, Universiti Teknikal Malaysia Melaka (UTeM) for providing the research grant FRGS/1/2014/TK03/FKE/02/F00208, PJP/2016/FKE/H15/S01478 and FRGS/1/2015/TK04/FKE/02/F00260.

REFERENCES

1. Chapman, S. J. *Electric Machinery Fundamental (Power & Energy)*, 4th Edition, 533–557, McGraw Hill Higher Education, Singapore, 2005.
2. Feng, C., S. Cui, and S. Chen, “Performance analysis of double-stator starter generator for the hybrid electric vehicle,” *IEEE Transactions on Magnetics*, Vol. 41, No. 1, 484–487, 2005.
3. Chau, K. T., Y. B. Li, and J. Z. Jiang, “Design and analysis of a stator-doubly-fed-doubly-salient permanent-magnet machine for automotive engines,” *IEEE Transactions on Magnetics*, Vol. 42, 3470–3472, 2006.
4. Liu, C., K. T. Chau, J. Z. Jiang, and L. Jian, “Design a new outer-rotor permanent magnet hybrid machine for wind power generation,” *IEEE Transactions on Magnetics*, Vol. 44, 1494–1497, 2008.
5. Norhisam, M., M. Norafiza, and C. Y. Sia, “Double stator type permanent magnet generator,” *Proceeding of 2009 Student Conference on Research and Development (SCORED)*, 316–319, 2009.
6. Wang, Y., S. Niu, and W. Fu, “Electromagnetic performance analysis of novel flux-regulatable permanent magnet machines for wide constant-power speed range operation,” *Energies*, Vol. 8, 13971–13984, 2015.
7. Norhisam, M., S. Ridzuan, R. N. Firdaus, C. V. Aravind, H. Wakiwaka, and M. Nirei, “Comparative evaluation on power-speed density of portable permanent magnet generator for agriculture applications,” *Progress In Electromagnetics Research*, Vol. 129, 345–363, 2012.
8. Zheng, P., Q. Wu, J. Bai, C. Tong, and Z. Song, “Analysis and experiment of a novel brushless double rotor machine for power-split hybrid electrical vehicle applications,” *Energies*, Vol. 6, 3209–3223, 2009.
9. Vaithilingam, C. A., N. Misron, M. R. Zare, I. Aris, and M. H. Marhaban, “Computation of electromagnetic torque in a double rotor switched reluctance motor using flux tube methods,” *Energies*, Vol. 5, 4008–4026, 2012.
10. Norhisam, M., R. Suhairi, M. Norafiza, M. A. M Radzi, I. Aris, M. Nirei, and H. Wakiwaka, “Comparison on performance of a single phase and three phase double stator type permanent magnet generator,” *Asia-Pacific Symposium on Applied Electromagnetics and Mechanics, Kuala Lumpur*, 231–234, 2010.
11. Norhisam, M., M. Norafiza, and C. Y. Sia, “Double stator type permanent magnet generator,” *Proceeding of 2009 Student Conference on Research and Development (SCORED 2009)*, 316–319, UPM Serdang, Malaysia, Nov. 16–18, 2009.
12. Norhisam, M., M. Norafiza, M. Nirei, H. Wakiwaka, M. Syafiq, and I. Aris, “Comparison on performance of a single and double stator of a slot-less permanent magnet generator,” *21st Symposium on Electromagnetics and Dynamics*, 561–564, 2009.
13. Raja, N. F., M. Norhisam, A. V. Chockalingam, M. Nirei, and W. Hiroyuki, “Improvement of energy density in single stator interior permanent magnet using double stator topology,” *Mathematical Problems in Engineering*, Vol. 2014, 15 pages, Article ID 787382, 2014.
14. Zhang, D., S. Niu, K. T. Chau, J. Z. Jiang, and C. Liu, “Design and analysis of a double-stator cup-rotor PM integrated-starter-generator,” *Conference Record of the 2006 IEEE Industry Applications Conference Forty-First IAS Annual Meeting*, 20–26, 2006.
15. Niu, S., K. T. Chau, J. Z. Jiang, and C. Liu, “Design and control of a new double-stator cup-rotor permanent-magnet machine for wind power generation,” *IEEE Transactions on Magnetics*, Vol. 43, 2501–2503, 2007.
16. Niu, S., S. L. Ho, and W. N. Fu, “A novel direct-drive dual-structure permanent magnet machine,” *IEEE Transactions on Magnetics*, Vol. 46, 2036–2039, 2010.
17. Wang, Y., M. Cheng, Y. Fan, and K. T. Chau, “A double-stator permanent magnet brushless machine system for electric variable transmission in hybrid electric vehicles,” *IEEE Vehicle Power and Propulsion Conference*, 1–5, 2010.
18. Feng, C., S. Cui, and C. Kang, “Performance analysis of double-stator starter generator for the hybrid electric vehicle,” *12th Symposium on Electromagnetic Launch Technology*, 499–502, 2004.

19. Alam, S. S., N. A. Omar, M. S. B. Ahmad, H. R. Siddiquei, and S. M. Nor, "Renewable energy in malaysia: Strategies and development," *Environmental Management and Sustainable Development*, Vol. 2, 51–66, 2013.
20. Firdaus, R. N., R. Suhairi, S. Farina, K. A. Karim, and Z. Ibrahim, "Improvement of power density spoke type permanent magnet generator," *IEEE PEDS*, 197–201, 2015.
21. Kim, S., II, J. Cho, S. Park, T. Park, and S. Lim, "Characteristics comparison of a conventional and modified spoke-type ferrite magnet motor for traction drives of low-speed electric vehicles," *IEEE Transactions on Industry Applications*, Vol. 49, 2516–2523, 2013.
22. Kim, K.-C. and J. Lee, "The dynamic analysis of a spoke-type permanent magnet generator with large overhang," *IEEE Transactions on Magnetics*, Vol. 41, 3805–3807, 2005.
23. Wang, J., W. Wang, G. W. Jewell, and D. Howe, "Design of a miniature permanent-magnet generator and energy storage system," *IEEE Transactions on Industrial Electronics*, Vol. 52, No. 5, 1383–1390, 2005.
24. Boughrara, K., R. Ibtouen, and N. Takorabet, "Analytic calculation of magnetic field and electromagnetic performances of spoke type IPM topologies with auxiliary magnets," *International Conference on Electrical Machines (ICEM)*, Vol. 7, 51–57, 2014.
25. Hirata, K., Y. Kagami, M. Yanosaka, Y. Ishihari, and T. Todaka, "Thrust calculation of linear pulse motors using a combined technique employing the finite element method and the permeance analysis method," *IEEE Transactions on Magnetics*, Vol. 28, No. 2, 1394–1397, 1992.
26. Delforge, C. and B. Lemaire-Semail, "Induction machine modeling using finite element and permeance network methods," *IEEE Transactions on Magnetics*, Vol. 31, No. 3, 2092–2095, 1995.
27. Wang, X., Q. Li, S. Wang, and Q. Li, "Analytical calculation of air-gap magnetic field distribution and instantaneous characteristics of brushless DC motors," *IEEE Transactions on Energy Conversion*, Vol. 18, No. 3, 424–432, 2002.